

Submitted to  
14<sup>th</sup> Symposium on Thermophysical Properties  
and the  
International Journal of Thermophysics

**Optical Properties of Polyimide Films in the Infrared**

P. A. Kawka<sup>1</sup> and R. O. Buckius<sup>2, 3</sup>

---

<sup>1</sup> Research Assistant, Department of Mechanical and Industrial Engineering, University of Illinois at Urbana-Champaign, Urbana, Illinois 61801, U.S.A.

<sup>2</sup> Professor and Head, Department of Mechanical and Industrial Engineering, University of Illinois at Urbana-Champaign, Urbana, Illinois 61801, U.S.A., corresponding author.

<sup>3</sup>To whom correspondence should be addressed.

## **ABSTRACT**

This study determined infrared optical constants of polyimide film in the spectral range between  $2000\text{ cm}^{-1}$  and  $7000\text{ cm}^{-1}$  using a five-oscillator Lorentz model. Model parameters are presented in addition to the derived values of the complex refractive index and dielectric constant. The parameters were obtained using electromagnetic theory for thin films to model reflectivity data from two thickness film samples ( $5.17\text{ }\mu\text{m}$ ,  $12.4\text{ }\mu\text{m}$ ) on gold substrates examined at two different incident angles. Measurements were taken using a polarizable reflectometer device in a Fourier Transform Infrared (FT-IR) Spectrometer. The real part of the refractive index,  $n$ , is shown to be about 1.67 while the imaginary part,  $k$ , is less than 0.01 over the spectral range examined. Results are consistent with findings of other experimenters, and new data presented here show that polarization effects on the thin film layers are predictable from the presented model.

**KEY WORDS:** Fourier transform infrared spectrometer (FT-IR); Lorentz model; optical constants; polarization; polyimide films; radiative properties; reflectivity; refractive index.

## 1. INTRODUCTION

Thin film surfaces are common in engineering applications affecting thermal transfer and optical phenomena in a wide range of scenarios from the oxide layers that form over most metals to manufacturing processes in micro-systems. In the rapidly growing fields of integrated circuits (ICs) and micro-electro-mechanical systems (MEMS), thin films play an important role in creating stress buffers, acting as dielectric materials, serving as optical waveguides, protecting and coating junctions, and forming structures[1-4]. One of the important materials used to create these coatings is polyimide. Liquid polyimide precursors can be easily applied to a variety of substrates, manipulated using photoresists, etching techniques, and photolithography and cured to provide a solvent resistant film structure useful for a variety of applications.

Because of its unique optical, electrical, and mechanical properties, several researchers have characterized polyimide for use in experiments and other practical uses. Some researchers have characterized polyimide properties for applications in liquid crystal displays (LCDs). The planar orientation of the long chain polymers in spun polyimide films results in a small degree of negative birefringence. This property has been investigated by Li, et al. [5] in the visible range to extend the viewing angles of twisted nematic LCDs. The application of negative birefringent polyimide compensates for the positive birefringence inherent in the liquid crystal. Other studies of polyimide for LCD application focus on the effect of film rubbing to orient the polyimide molecules which in turn allows alignment of the liquid crystal molecules when the crystals are applied. Sakamoto et al. [6] and Lavers [7] have studied polyimide films using IR spectroscopy and attenuated total reflection (ATR) spectroscopy, respectively, to

characterize how film rubbing affects the optical properties, molecular alignment, and surface roughness.

Polyimide optical properties have also been examined in the soft x-ray region from transmission measurements with Kramers-Kronig analysis and multiple angle reflection measurements [8]. The motivation in this study was to carefully characterize errors in those optical property determination processes, compare two different methods for finding optical constants, and provide useful x-ray optical properties for polyimide applicable to x-ray lithography.

Finally, optical property characterization of polyimide in the infrared between 500  $\text{cm}^{-1}$  and 6000  $\text{cm}^{-1}$  has been performed by Zhang, et al. [9] using unpolarized FT-IR transmission measurements of films of varying thicknesses to facilitate design in filters and optoelectronic application. Minimization of the RMS error and Lorentz modeling were both used to determine optical constants.

In this work, Fourier Transform Infrared (FT-IR) Spectroscopy is used to measure the bi-directional reflectivity ( $\rho''$ ) of polyimide films on gold substrates in the infrared. The optical constants of cured polyimide are determined in the infrared region between 2000 and 7000  $\text{cm}^{-1}$  (5 and 1.4  $\mu\text{m}$ ) using a Lorentz model to characterize the absorption bands. The effect of polarizing the incident and reflected radiation is examined to determine if the generally planar orientation of the molecules in the spun films significantly affects the properties. The model parameters are reported that minimize the RMS error between the experimental reflectivity measurements and the computed theoretical reflectivity from optical constants.

## **2. EXPERIMENTS**

### **2.1 Surface Fabrication**

To determine the optical property characteristics of PI2723, two thin film test samples were fabricated in the cleanroom facilities of the University of Illinois Microelectronics Lab. Uncoated, unprotected 1” circular gold mirrors were obtained from Melles Griot (part# 02MFG015045) and served as substrates for the thin film samples. To prepare the samples, each mirror substrate was first cleaned using acetone followed by isopropyl alcohol followed by de-ionized water. Any remaining water was blown from the surface using filtered air, and the sample was placed briefly on a 110°C hotplate to finish drying. On each substrate, a small piece of tape was placed on the edge to serve as a mask to remove a small portion of subsequent layers of polyimide and allow easy measurement of the film thickness.

Each substrate was placed on a centripetal spinner set to run for 45 seconds at 2000RPM. Five drops of PI2723 were then placed in the center of the sample using an eyedropper before the spinner was started. Soft curing of the samples on a hot plate followed the spinning procedure and lasted 4 minutes at 75°C. To create a thicker film layer, the above steps were repeated to add a second coating of film to one of the samples. At this point the pieces of masking tape were removed from the samples and the photosensitive PI samples were UV exposed at an intensity of about 2 to 3 mW/cm<sup>3</sup> to provide a 200 mJ/cm<sup>3</sup> dosage. The procedure presented closely follows the directions provided by HD Microsystems [10] for the usage of PI2723.

The final step in the sample preparation was an approximately 7 hour vacuum annealing process to hard cure the samples to a repeatable condition. First the samples

were placed on a 60°C hotplate open to the room air that ramps up to 150°C over 45 minutes. Once at 150°C, the samples were baked for 30 minutes before the hot plate ramped up to 300°C over 75 minutes. Once at 300°C, a glass dome was placed over the sample and a roughing pump was used to bring the pressure down to about 500  $\mu$ -atm. A very low flow N<sub>2</sub> bleed was turned on to prevent roughing pump oil from diffusing into the chamber. After baking for 30 minutes at 300°C in the vacuum, the hot plate was ramped up to 450°C over 75 minutes. Once at 450°C, the samples were baked for 45 minutes. Finally, the samples were allowed to cool in the vacuum environment to 60°C over about 2 hours before being removed.

After the vacuum annealing, a Tencor Instruments Alpha Step 200 physical profilometer was used to measure the film thicknesses for each sample by measuring the height of the step creating by the masking process. The single layer sample was found to have a film height (h) of  $5.17 \pm 0.20 \mu\text{m}$ , and the double coated sample had a film thickness of  $12.5 \pm 0.8 \mu\text{m}$ . The samples were then stored in a desiccated environment to prevent excess water absorption by the polyimide films.

## **2.2 Reflection Measurements**

To determine the optical constants of the PI2723 material, a Nicolet Magna-IR<sup>TM</sup> 750 Fourier Transform Infrared (FT-IR) Spectrometer was used with a reflectometer apparatus to measure the in-plane reflectivity of the samples. The reflectometer system is based on a modified Seagull<sup>TM</sup> variable-angle reflectivity accessory from Harrick Scientific Corporation and allows collection of in-plane bi-directional reflectivity data. Polarizers are fixed on the inlet and outlet ports to allow selection of polarized radiation parallel or perpendicular to the plane of incidence. Using a liquid nitrogen cooled

mercury cadmium telluride (MCT) quantum detector and an air-cooled Ever-Glo™ source operating at 1500K, the FT-IR spectrometer is capable of measuring the reflected energy from the surface as a function of wavenumber ranging from about 650 cm<sup>-1</sup> to 7000 cm<sup>-1</sup> (15.38 μm to 1.43 μm). For all measurements reported in this research, 256 spectral scans were averaged with a resolution of 32 cm<sup>-1</sup>. The incident and reflected solid angles for the system are known to be approximately 3° in this work [11].

An uncoated gold mirror identical to the filmed sample substrates was used as the reference material and was assumed to have known spectral dependent optical properties,  $n$  and  $k$ , given by Brewster [12]. To be able to use the gold properties at discrete values over a large range of wavenumbers, the data was fit using power law relationships that represented the  $n$  and  $k$  data points with a maximum error less than 3.2% and an average error less than 1.3%.

To determine the optical properties of the PI2723 thin films, reflection data of each surface was taken for incident angles of 30° and 45° and for ss (entry and exit perpendicular to plane of incidence) and pp (entry and exit parallel to plane of incidence) polarizations. Cross polarization (sp and ps) were also examined and shown to contain a negligible amount of energy that was below the measurement threshold of the FT-IR system. Using a relative method, the bi-directional spectral reflectivities of samples can be determined using the following equation [11]:

$$\rho''_{\lambda}(\Omega_i, \Omega_r) = \rho''_{\lambda, \text{ref}}(\Omega_i, \Omega_r) \frac{V_m}{V_{\text{ref}}} \quad (1)$$

All measurements were performed for the same incident and reflected solid angles.

### 3. ANALYSIS

For a general surface, bi-directional reflectivity ( $\rho''$ ) is the fundamental characterization of its reflection characteristics. It is defined as the ratio of  $\pi$  times the reflected intensity over the incident partial flux and is, in general, a function of wavelength and the incident and reflected angles. It can be expressed as

$$\rho''_{\lambda}(\Omega_i; \Omega_r) = \frac{\pi I_{\lambda_r}(\Omega_r)}{I_{\lambda_i}(\Omega_i) \cos \theta_i d\Omega_i} \quad (2)$$

where  $I$  is intensity,  $\Omega$  is a solid angle,  $\theta$  is a polar angle,  $\lambda$  is a wavelength, and the subscripts  $i$  and  $r$  denote incident and reflected, respectively [12].

In this study, both the film-coated substrates and reference mirror are assumed to produce specular reflections in the infrared region. For ideal specular reflection, bi-directional reflectivity  $\rho''$  can be related to hemispherical reflectivity using

$$\rho''_{\lambda} = \pi \rho'_{\lambda} \frac{\delta(\theta_r - \theta) \delta(\phi - \phi_r + \pi)}{\cos \theta \sin \theta} \quad (3)$$

where  $\delta$  is the Dirac delta function and  $\phi$  is the azimuthal angle. Assuming for the experiments that the incident energy is reflected nearly specularly and all captured in the system's solid angle about the reflected angle, it is possible to combine Eqs. (1) and (2) to allow direct computation of the hemispherical reflectivity using

$$\rho'_{\lambda}(\Omega_i, \Omega_r) = \rho'_{\lambda, \text{ref}}(\Omega_i, \Omega_r) \frac{V_m}{V_{\text{ref}}} \quad (4)$$

where  $V_m$  and  $V_{\text{ref}}$  are the experimentally measured voltages for sample and the reference.

The assumption of nearly specular reflection allows comparison with electromagnetic theory results for layered media. Layer reflectivity [12,13] is found using



$$\rho'_{\text{film}} = \left| \frac{r_{12} + r_{23}e^{-i2\beta}}{1 + r_{12}r_{23}e^{-i2\beta}} \right|^2 \quad (5)$$

where

$$\tilde{\beta} = \frac{2\pi \tilde{n}_2 h \cos \tilde{\theta}_2}{\lambda_0} \quad (6)$$

and the Fresnel coefficients or complex amplitude ratios are given by

$$r_{ab\parallel} = \frac{\tilde{n}_b \cos \tilde{\theta}_a - \tilde{n}_a \cos \tilde{\theta}_b}{\tilde{n}_b \cos \tilde{\theta}_a + \tilde{n}_a \cos \tilde{\theta}_b} \quad (7)$$

$$r_{ab\perp} = \frac{\tilde{n}_a \cos \tilde{\theta}_a - \tilde{n}_b \cos \tilde{\theta}_b}{\tilde{n}_a \cos \tilde{\theta}_a + \tilde{n}_b \cos \tilde{\theta}_b}. \quad (8)$$

In Eqs. (5) and (6),  $r$  is the interface reflectivity and the subscripts 1, 2 and 3 stand for the different media with 1 representing air having purely real refractive index  $n=1$ , 2 representing the polyimide film, and 3 representing the gold substrate. The subscripts  $a$  and  $b$  represent different choices of material numbers (1, 2 or 3) to describe a reflection or coefficient when a wave is incident from medium  $a$  to medium  $b$ . The symbol  $\tilde{n}$  is the complex refractive index given as  $n-ik$ , and  $\tilde{\theta}$  is a complex representation of the angle of propagation in the media. For a medium with no absorption ( $k=0$ ),  $\theta$  is the angle of propagation in the medium measured from the normal. The propagation angles in the different media are related by Snell's Law as

$$\tilde{n}_a \sin \tilde{\theta}_a = \tilde{n}_b \sin \tilde{\theta}_b. \quad (9)$$

In addition, the complex refractive index,  $\tilde{n}$ , can be represented equivalently by the complex dielectric constant given by

$$\tilde{\epsilon}_r = \epsilon_r' - i\epsilon_r'' = \tilde{n}^2 \quad (10)$$

where  $\epsilon_r'$  and  $\epsilon_r''$  are the real and imaginary part of the relative permittivity.

In general, the optical constants of a material vary spectrally and often can be modeled using a damped oscillator or Lorentz model. Under the assumptions that a material is composed of charged particles held in place by isotropic elastic forces, and affected by isotropic linear damping forces, it can be shown that for a single oscillator

$$\tilde{\epsilon}_r = \tilde{n}^2 = 1 + \frac{\omega_p^2}{\omega_0^2 - \omega^2 + i\gamma\omega} \quad (11)$$

where  $\omega_p$  is the plasma frequency,  $\omega_0$  is the oscillator frequency, and  $\gamma$  is the relaxation frequency [12, 14]. A multiple oscillator model of this type is used to characterize the spectral optical constants of polyimide in the infrared. The oscillator model in Eqs. (10) and (11) provides the dielectric constants given by

$$\epsilon_r' = n^2 - k^2 = n_e^2 + \sum_{j=1}^5 \frac{\omega_{pj}^2 (\omega_{0j}^2 - \omega^2)}{(\omega_{0j}^2 - \omega^2)^2 + \gamma_j^2 \omega^2} \quad (12)$$

$$\epsilon_r'' = 2nk = \sum_{j=1}^5 \frac{\omega_{pj}^2 \gamma_j \omega}{(\omega_{0j}^2 - \omega^2)^2 + \gamma_j^2 \omega^2} \quad (13)$$

and the indices of refraction given as

$$n = \left[ \frac{\epsilon_r' + \sqrt{\epsilon_r'^2 + \epsilon_r''^2}}{2} \right]^{\frac{1}{2}} \quad (14)$$

$$k = \left[ \frac{-\epsilon_r' + \sqrt{\epsilon_r'^2 + \epsilon_r''^2}}{2} \right]^{\frac{1}{2}}. \quad (15)$$

To obtain the optical constants of the polyimide film, the measured reflectivity properties and are used to determine the refractive index using the electromagnetic theory presented in Eqs. (5) through (9). The film reflectivity prediction from those equations is for a single specular angle of incidence and reflection, so results were averaged over a

solid angle of  $3^\circ$  to correspond to the conditions of the experimental data as closely as possible. Spectral averaging over  $32 \text{ cm}^{-1}$  was not performed because the reflectivity does not change very significantly within each  $32 \text{ cm}^{-1}$  interval over the spectral region from 2000 to  $7000 \text{ cm}^{-1}$ , and the spectral averaging would not have a significant effect on the accuracy of the results (maximum single data point change of  $<2\%$ ).

The eight sets of data obtained from the three independent parameters of incident angle ( $30^\circ$  or  $45^\circ$ ), film thickness ( $5.17 \text{ }\mu\text{m}$  or  $12.5 \text{ }\mu\text{m}$ ), and polarization (pp, ss) were reduced to four sets of data by averaging the pp and ss polarizations. From the four sets of reflectivity data, it was observed that no significant absorption bands appeared between  $4000$  and  $7000 \text{ cm}^{-1}$ . Therefore, this region was used to assess and evaluate the values of the PI film thicknesses ( $h_1, h_2$ ) and the optical constant  $n_e$  (assuming  $k=0$ ) that predict the layer reflectivities that best fit the measured data. The subscript e represents an equivalent value that accounts for contributions to the refractive index from oscillators at frequencies lower than the region of interest that are not modeled.

The film thicknesses  $h_1$  and  $h_2$  were only allowed to vary within the range  $\pm 10\%$  of the experimental measured values to allow for the possibility of some error in measurement and the variability of height with position. The best fit of the data was obtained by varying the 4 parameters until the spectrally averaged RMS difference between the theoretical prediction and the experimental values was minimized. The values of  $h_1$  and  $h_2$  are  $5.17 \text{ }\mu\text{m}$  and  $12.4 \text{ }\mu\text{m}$  as noted in Table I.

With the film heights and high wavenumber (high frequency) optical constants evaluated, the spectral region between about  $2000$  and  $4000 \text{ cm}^{-1}$  was then examined to determine the spectral variation of  $n$  and  $k$  due to absorption bands in the film. To treat the absorption bands between  $2000$  and  $4000 \text{ cm}^{-1}$ , a five-oscillator Lorentz model was applied to the spectral region in a similar treatment to that performed by Zhang et al. [9] and Sakamoto [15]. The locations of the oscillators ( $\omega_{0i}$ ) were determined through a

combination of data inspection, reported values in the literature [16], and error minimization. At each oscillator location, the two remaining oscillator parameters  $\omega_p$  and  $\gamma$ , controlling the oscillator strength and width respectively, were varied to minimize the error in the prediction and are given in Table I. The theoretical reflectivity curve is derived from Eqs. (5) through (9), and the fitted optical properties from the oscillator model.

#### 4. RESULTS AND DISCUSSION

The experimental reflectivity data for the four cases examined ( $30^\circ$  and  $45^\circ$  incidence,  $5.17\ \mu\text{m}$  and  $12.4\ \mu\text{m}$  layer thicknesses) is compared to the reflectivity computed from the model results in Figs. 1 through 4. Each figure shows the model prediction and experimental results for ss, pp, and averaged polarizations. The maximum and average error between the reflectivity calculated from the model and experimental results for each case of averaged polarization are computed and given in Table II.

The error statistics from Table II indicate that the five-oscillator model well represents the experimental results on a spectrally averaged and polarization averaged basis from  $2000\ \text{cm}^{-1}$  to  $7000\ \text{cm}^{-1}$ . The spectrally averaged absolute error is less than 4% for all four cases, and the spectrally averaged RMS error is less than 0.045. The single data point maximum error is 29% and occurs in the case with  $30^\circ$  incidence on a  $12.4\ \mu\text{m}$  film. This error occurs at a wavenumber of  $2962\ \text{cm}^{-1}$  that is in the vicinity of an absorption band and is the general spectral region of the largest single point errors for both  $45^\circ$  incident cases as well. With the five-oscillator model result, the experimental data is well represented both in magnitude and trend. Any large changes in reflectivity due to absorption bands and the superimposed ripples from interference effects are

qualitatively captured by the theoretical curve fit, even though it is not able to predict all of the fine detail. Some overprediction and underprediction of the reflectivity does occur at the locations of the greatest property changes. In addition, in the spectral region from about  $4000\text{ cm}^{-1}$  to  $7000\text{ cm}^{-1}$  where no absorption bands are observed, the model has a relatively constant level of error. The model predicts a reflection that is about 4.5% too high for the  $5.17\text{ }\mu\text{m}$  samples and is about 2.5% too high for the  $12.4\text{ }\mu\text{m}$  samples. This systematic offset of difference between the experiments and the model are likely due to measurement errors in the FTIR system and assumptions made in the analysis. It is likely that small amounts of roughness in the film surface and minor shifts of the focal plane from using surfaces with varying film thickness cause the assumption of a flat specular film to be less accurate. Some energy is therefore not captured in the reflected solid angle resulting in experimental values lower than the predicted values. The increasing effect of film roughness and decreasing signal can be observed in Fig. 4(b) showing pp polarized reflection of the thicker and rougher two-layer sample. At higher wavenumbers (shorter wavelengths), the interference becomes less distinguishable and deviates from its smooth periodicity.

The spectral variation of the optical properties based on the model is presented in Fig. 5 as  $n$  and  $k$  and in Fig. 6 as  $\epsilon_r'$  and  $\epsilon_r''$ . From the variations in  $n$  or  $\epsilon_r'$  and the peaks in  $k$  or  $\epsilon_r''$ , the contributions of four of the five oscillators are clearly distinguished. The fifth oscillator exists at a location just below  $2000\text{ cm}^{-1}$  and is responsible for the initial increase in  $n$  and  $\epsilon_r'$  and the initial decrease of  $k$  and  $\epsilon_r''$ . The real part of the refractive index and dielectric constant,  $n$  and  $\epsilon_r'$ , do not vary significantly in the spectral region from  $2000\text{ cm}^{-1}$  to  $7000\text{ cm}^{-1}$ . Both begin at a minimum value, increase rapidly and level

off to a steady value corresponding to  $n_e=1.68$  that is less than 7% greater than the initial value. Small variations occur consisting of an increase followed by a decrease followed by an increase at the locations of the oscillators. For the complex part of the refractive index and dielectric constant,  $k$  and  $\epsilon''$ , local peaks occur at the locations of the oscillators and the maximum value occurs at  $2919\text{ cm}^{-1}$  where the strongest oscillator between  $2000\text{ cm}^{-1}$ - $7000\text{ cm}^{-1}$  exists. At high wavenumbers, the complex part drops to a very small value approaching 0 for increasing wavenumbers.

Overall, the results presented are consistent with findings of other researchers. The values of  $n$  varying from 1.64 to 1.68 over the spectral range from  $2000\text{ cm}^{-1}$  to  $7000\text{ cm}^{-1}$  are between the value of 1.59 obtained by Saito et al. [17] and the values of 1.73 to 1.75 in the spectral region between  $2500\text{ cm}^{-1}$  to  $6000\text{ cm}^{-1}$  obtained by Zhang, et al. [9]. The imaginary part of the refractive index was less than 0.01 over the entire region examined and was less than 0.001 between  $4000\text{ cm}^{-1}$  and  $7000\text{ cm}^{-1}$ . Peaks occurred at the location of the absorption bands as indicated on Fig. 5.

Even though the Lorentz model was developed using the averaged polarization effects, the values of  $n$  and  $k$  it provides also accurately predict polarized reflection distributions. The reflectivity values for the polarized cases are obtained again using the electromagnetic theory for thin films (Eqs. (5) through (9)). Even though the electromagnetic film theory development assumes homogeneous and isotropic optical properties within the film, the results are correct to within the same error levels obtained for the averaged polarization case. This result indicates that even though the polyimide polymer material has long chain molecules and has been shown to demonstrate anisotropic optical properties in other studies by Hardaker, et al. [3], Sakamoto et al. [6],

Lavers, et al. [7], and Goeschel, et. al. [18], these effects in spin coated, planar layers are small when compared with the spectral variation of the optical properties.

Overall, possible errors that affect the accuracy and applicability of the model presented are numerous. First, the properties of the gold coated substrate were not directly measured but came from tabulated data. Differences between the actual substrate properties and the tabulated properties used are unknown but should not have a large affect on the results because model parameters were derived based on reflectivity calculations. Because the optical properties of gold in the infrared lead to a very high and a relatively constant reflectivity, error from the characterization of the gold should not be very significant. Uncertainties also exist in the preparation and characterization of the polyimide films. Any roughness in the film layer causes some energy to be reflected off-specular that may not be collected in the solid angles of the reflectometer. This non-ideality would result in experimental reflectivities lower than those being predicted by theory for an equivalent set of parameters. In addition, polyimides have a complex chemical nature, and although measures were taken to fully cure the polyimide at high temperature in a vacuum oven to produce a repeatable condition, processing, storage, and aging of a film should affect it properties. Finally, uncertainties introduced simply from the use of the FT-IR system described have been determined to be less than 10% [11].

## **5. CONCLUSIONS**

This examination provides parameters for a five-oscillator Lorentz model of the thin film optical properties of PI2723 in the infrared from  $2000\text{ cm}^{-1}$  to  $7000\text{ cm}^{-1}$  when it is prepared using the standard procedures. Experimental reflectivity measurements of a

polyimide film over gold were taken using FT-IR spectroscopy. Model parameters were computed through minimization of the average spectral RMS error between experimental results in four different cases and the theoretical film reflectivity computed using Fresnel relations, electromagnetic theory, and the model parameters. The low values of average, RMS, and maximum error indicate the accuracy of the model. Polarization effects on the optical properties of spin-coated films are shown to be less significant than spectral variations in the optical properties.

## **ACKNOWLEDGEMENTS**

The research was supported, in part, by the National Science Foundation (NSF CTS 95-31772) and utilized the University of Illinois Microelectronics Lab facilities for sample preparation. The polyimide used in this work was obtained from the BioMEMS group headed by Professor David J. Beebe.



## REFERENCES

1. P.Y. Wong, B.D. Heilman, and I.N. Miaoulis, *Microscale Heat Transfer*, 291:27, (1994).
2. A.R. Abramson and C. L. Tien, *Microscale Therm. Eng.*, 3:229, (1999)
3. S.S. Hardaker, S. Moghazy, C. Y. Cha, and R. J. Samuels, *J. Polym. Sci. Pol. Phys.*, 31:1951, (1993).
4. K. R. Ha and J. L. West, *Mol. Cryst. Liq. Cryst.*, 323:129, (1998)
5. B. Li, T. He, and M. Ding, *Thin Solid Films*, 320:280, (1998).
6. K. Sakamoto, R. Arafune, S. Ushioda, *Applied Spectroscopy*, 51:541, (1997).
7. C. R. Lavers, *Thin Solid Films*, 289:133, (1996)
8. R. Wolf, H. G. Birken, and C. Kunz, C., *Appl. Opt.*, 31:7313 (1992).
9. Z. M. Zhang, G. Lefever-Burton, and F. R. Powell, *Int. J. Thermophys.*, 19:905, (1998).
10. HD Microsystems<sup>TM</sup>, Pyralin<sup>®</sup> PI2720 Processing Guidelines, (1998), pp. 1-16.
11. J. N. Ford, K. Tang, and R.O. Buckius, *J. Heat Transfer*, 117:955, (1995).
12. M. Q. Brewster, Thermal Radiative Transfer And Properties, (Wiley, New York, 1992), pp. 114-152, 504.
13. M. Born and E. Wolf, Principles of Optics, 6<sup>th</sup> ed. (Pergamon, Oxford, 1980), Chaps. 1, 13.
14. C. F. Bohren and D. R. Huffman, Absorption and Scattering of Light by Small Particles, (Wiley, New York, 1983), Chap. 9.
15. K. Sakamoto, R. Arafune, S. Ushioda, Y. Suzuki, and S. Morokawa, *J. Appl. Phys.*, 80:431, (1996).
16. H. Ishida, and M. T. Huang, *J. Polym. Sci. Pol. Phys.*, 32:2271, (1994).
17. Saito, M., Gojo, T., Kato, Y., and Miyagi, M., *Infrared Phys. Technol.*, 36:1125, (1995).
18. U. Goeschel, H. Lee, D. Y. Yoon, R. L. Siemens, B. A. Smith, and W. Volksen, *Colloid Polymer Sci.*, 272:1388, (1994).

## LIST OF FIGURES

Fig. 1(a)-(c). Comparison of Experimental and Predicted Layer Reflectivity for PI2723

Film with 5.17  $\mu\text{m}$  Thickness at 30° Incidence

Fig. 2(a)-(c). Comparison of Experimental and Predicted Layer Reflectivity for PI2723

Film with 5.17  $\mu\text{m}$  Thickness at 45° Incidence

Fig. 3(a)-(c). Comparison of Experimental and Predicted Layer Reflectivity for PI2723

Film with 12.4  $\mu\text{m}$  Thickness at 30° Incidence

Fig. 4(a)-(c). Comparison of Experimental and Predicted Layer Reflectivity for PI2723

Film with 12.4  $\mu\text{m}$  Thickness at 45° Incidence

Fig. 5. Optical Constants  $n$  and  $k$  vs. Wavenumber for PI2723 from Five-Oscillator

Model

Fig. 6. Dielectric Constants  $\epsilon_r'$  and  $\epsilon_r''$  vs. Wavenumber for PI2723 from Five-

Oscillator Model

**Table I: Parameters for Five-Oscillator Model**

$h_1 [\mu\text{m}] = 5.17$		$h_2 [\mu\text{m}] = 12.4$		$n_e = 1.68$	
	Oscillator 1	Oscillator 2	Oscillator 3	Oscillator 4	Oscillator 5
$\omega_p [\text{rad/s}]$	0.284	0.0611	0.0344	0.0541	0.0341
$\omega_o [\text{rad/s}]$	1.079	1.834	1.929	2.188	2.281
$\gamma [\text{rad/s}]$	0.0123	0.0799	0.0456	0.124	0.0432
$\eta [\text{cm}^{-1}]$	1717	2919	3070	3482	3630

**Table II: Maximum and Spectrally Averaged Error Between Model Prediction and  
Experimental Reflectivity for Averaged Polarizations**

Sample	Maximum absolute percent error [percent]	Spectrally averaged absolute percent error [percent]	Spectrally averaged RMS error
30°, 5.17 $\mu\text{m}$	8.52	3.95	0.0421
30°, 12.4 $\mu\text{m}$	28.7	3.20	0.0400
45°, 5.17 $\mu\text{m}$	13.4	3.49	0.0397
45°, 12.4 $\mu\text{m}$	19.4	3.24	0.0441

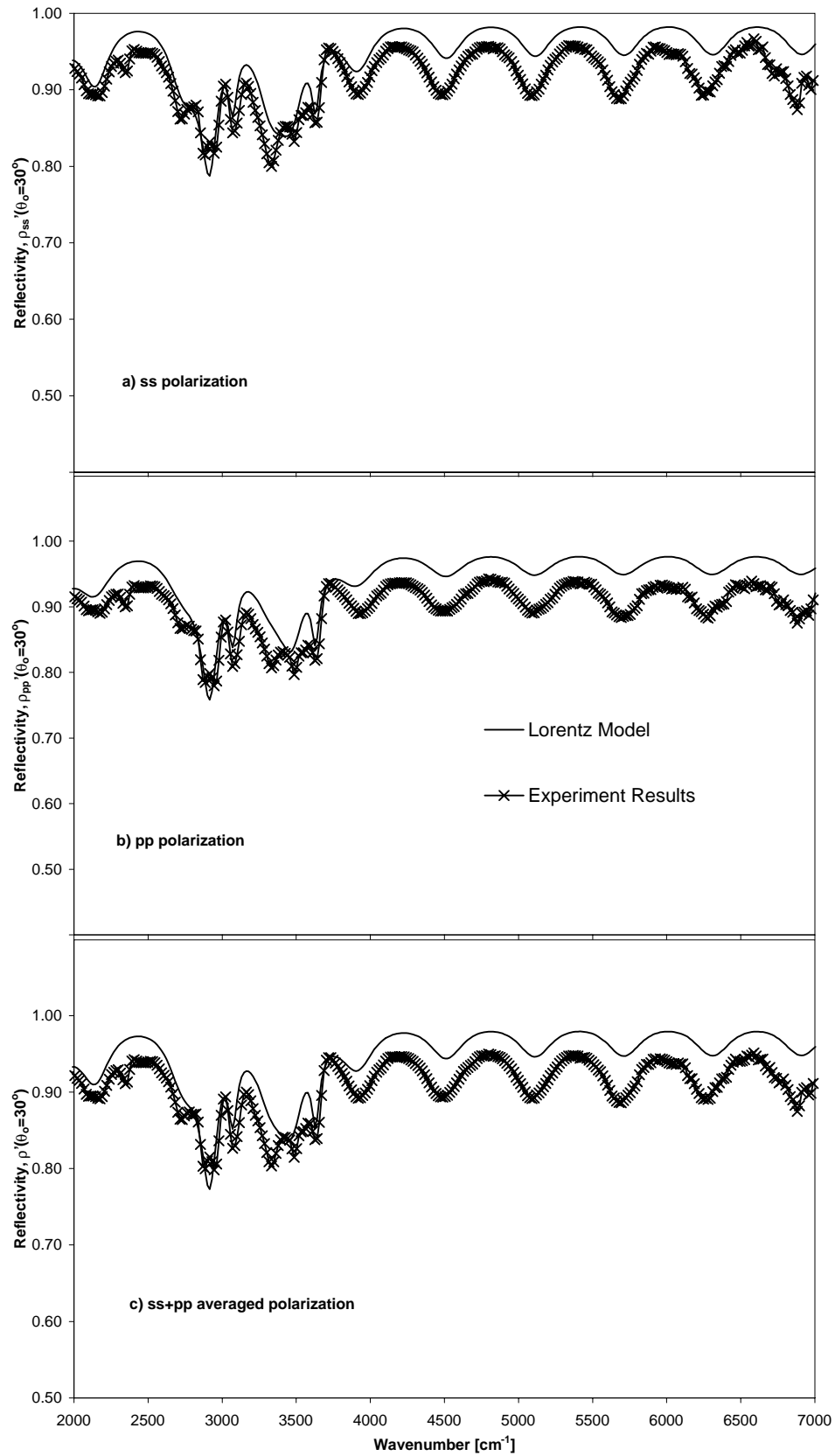


**Fig. 1(a)-1(c). Comparison of Experimental and Predicted Layer Reflectivity for PI2723 Film with 5.17  $\mu\text{m}$  Thickness at 30° Incidence**

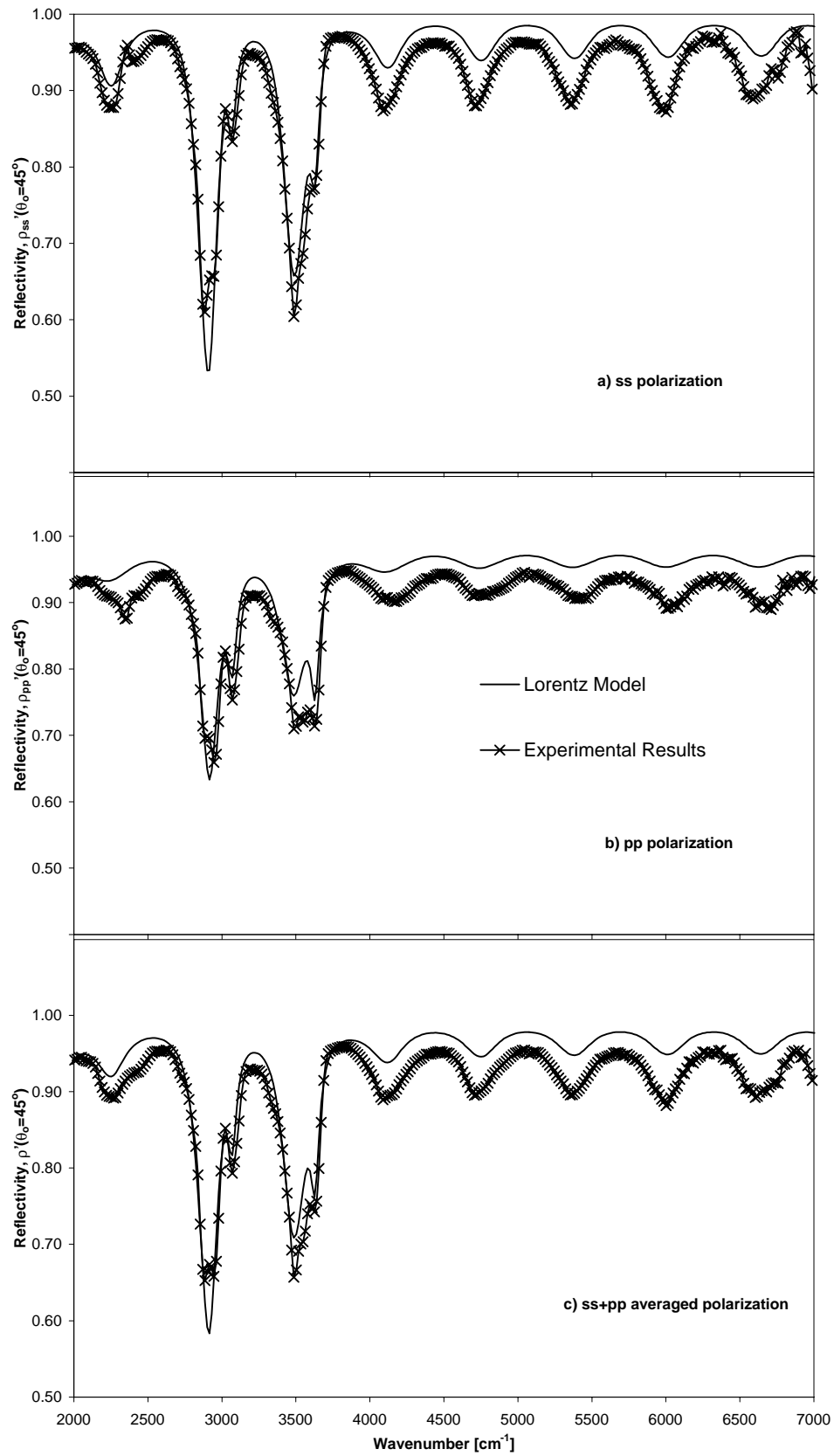


**Fig. 2(a)-2(c). Comparison of Experimental and Predicted Layer Reflectivity for PI2723 Film with 5.17  $\mu\text{m}$  Thickness at 45° Incidence**

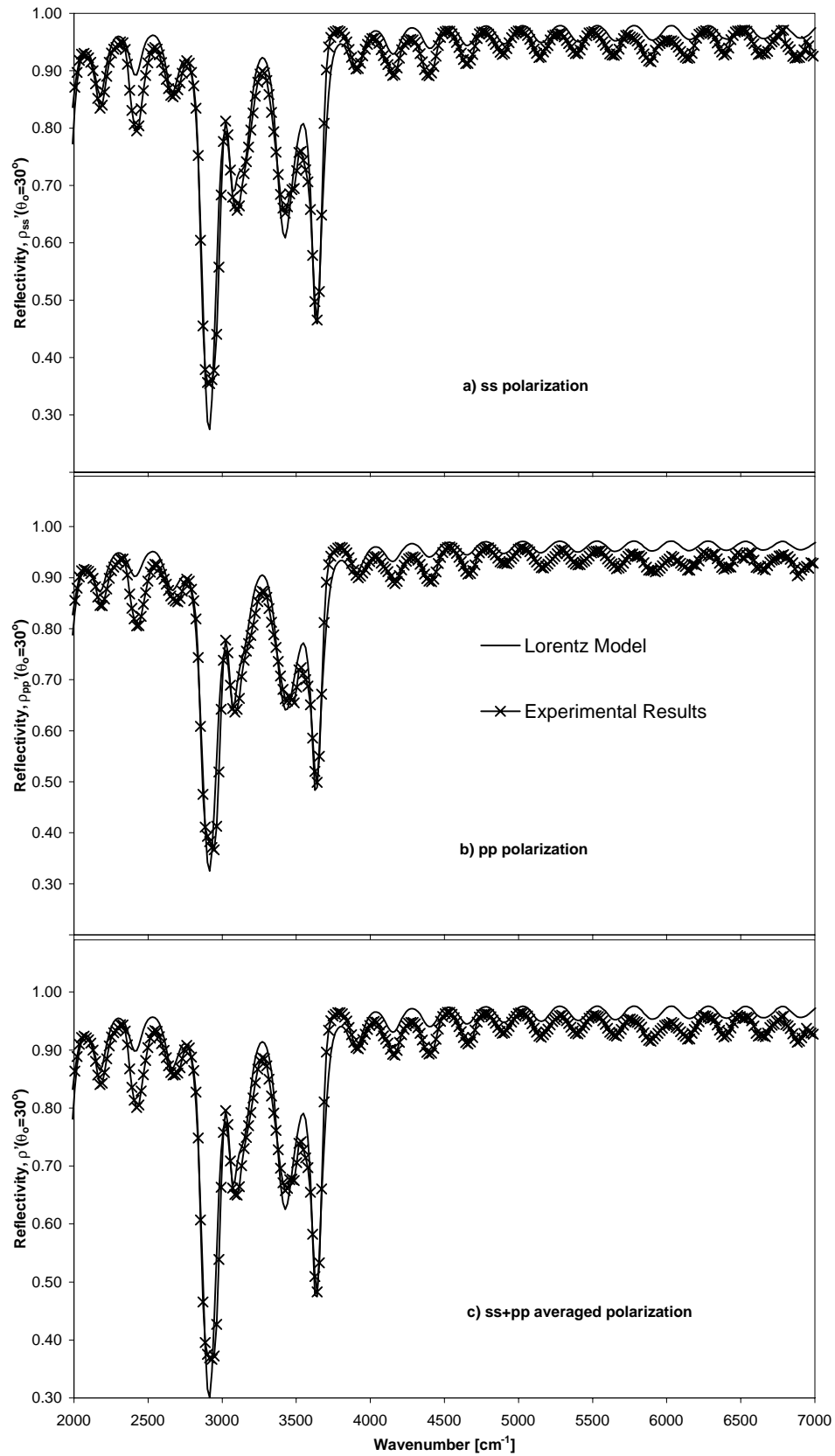


**Fig. 3(a)-3(c). Comparison of Experimental and Predicted Layer Reflectivity for PI2723 Film with 12.4 μm Thickness at 30° Incidence**

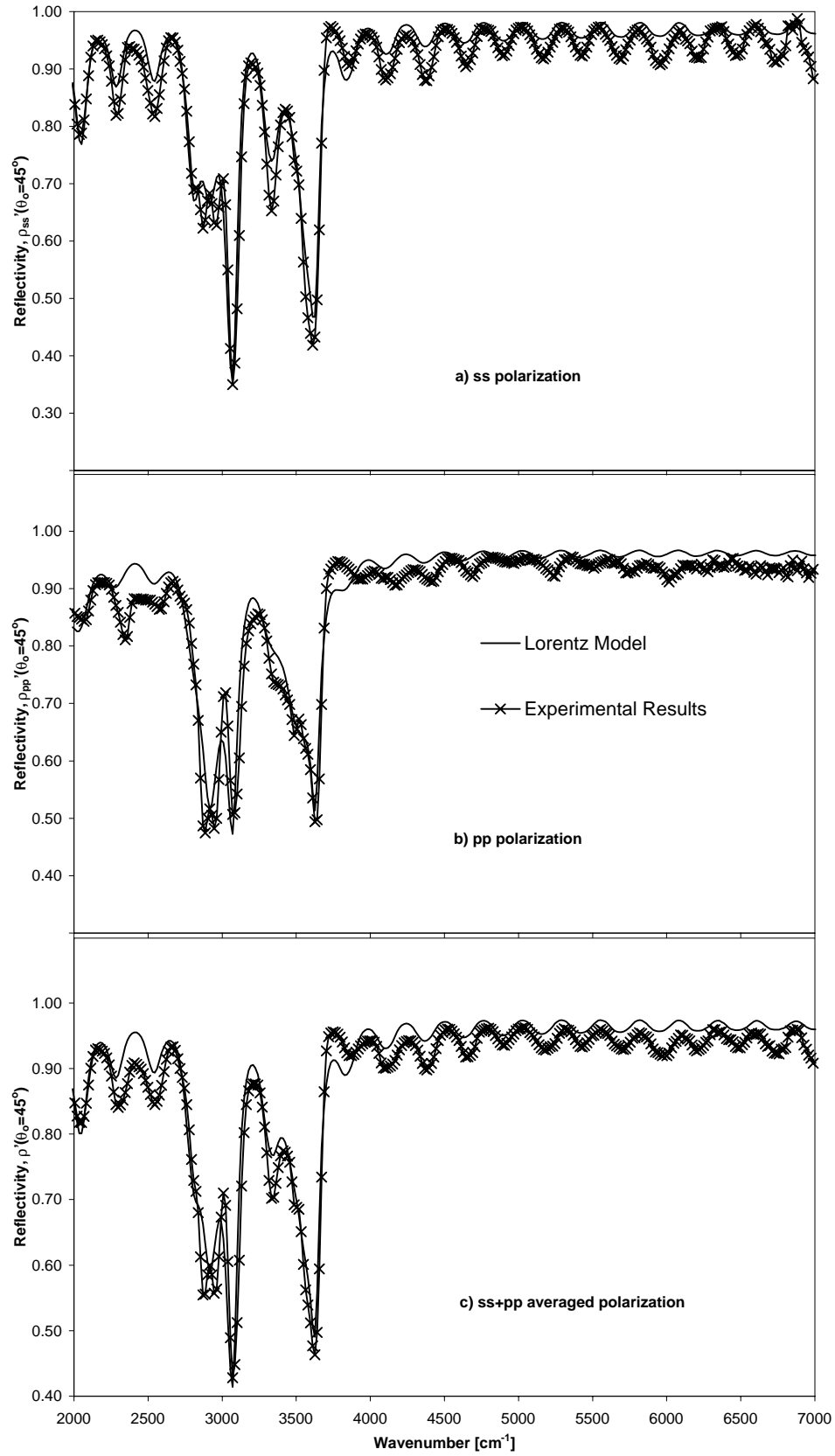


**Fig. 4(a)-4(c). Comparison of Experimental and Predicted Layer Reflectivity for PI2723 Film with 12.4  $\mu\text{m}$  Thickness at 45° Incidence**



Fig. 5. Optical Constants  $n$  and  $k$  for PI2723 using 5 Oscillator Model

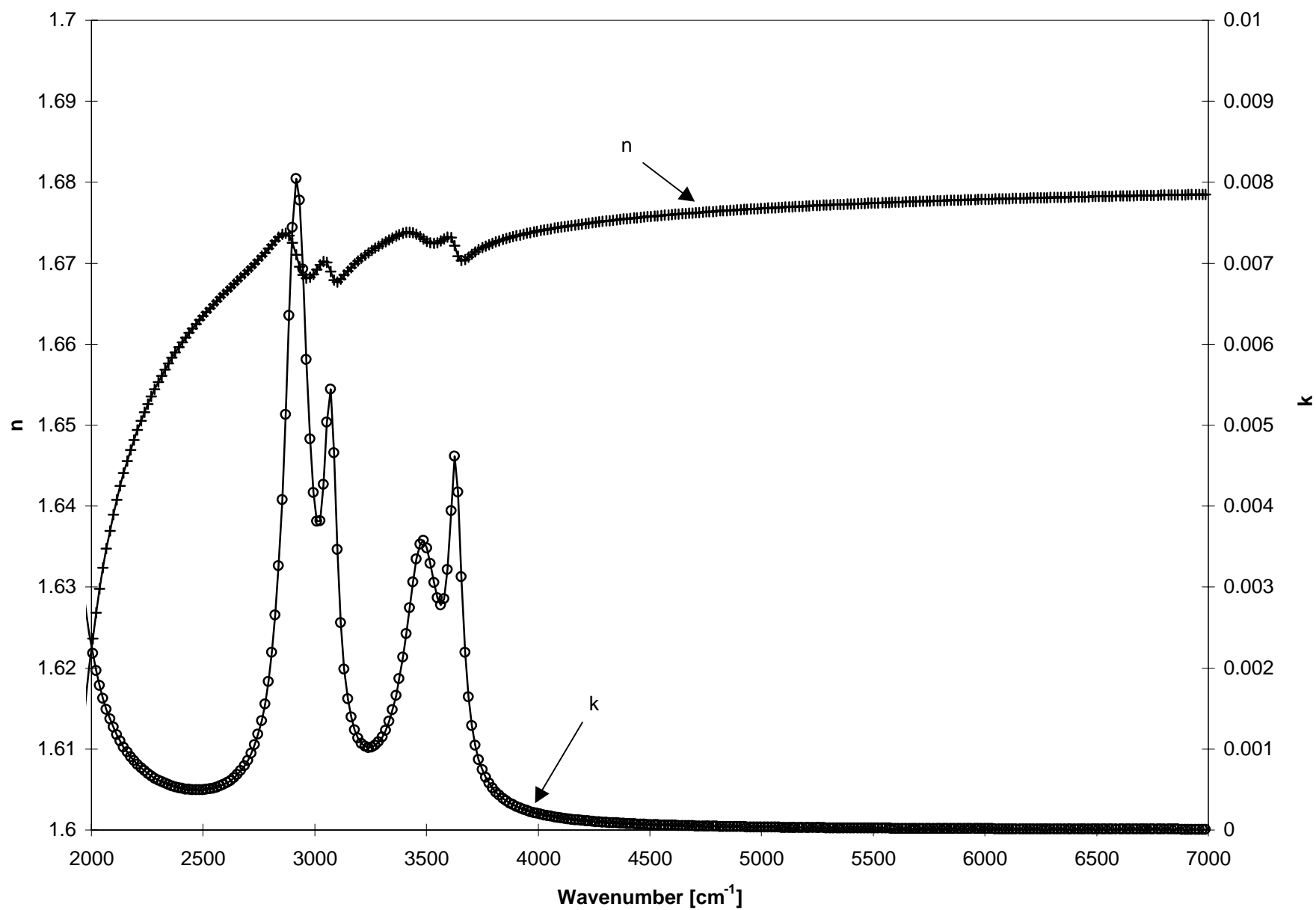


Fig. 6. Dielectric constants,  $\epsilon_r'$  and  $\epsilon_r''$  for PI2723 using 5 Oscillator Model

